Available online at www.sciencedirect.com
ScienceDirect
Journal of Solid State Chemistry 179 (2006) 3378–3384
JOURNAL OF SOLID STATE CHEMISTRY
www.elsevier.com/locate/jssc

Sm_2NiSn_4: The intermediate structure type between $ZrSi_2$ and $CeNiSi_2$

Zhong-Ming Sun, Da-Chun Pan, Xiao-Wu Lei, Jiang-Gao Mao*

State Key Laboratory of Structural Chemistry, Fujian Institute of Research on the Structure of Matter, Chinese Academy of Sciences, Fuzhou 350002, PR China

Received 18 May 2006; received in revised form 24 June 2006; accepted 2 July 2006
Available online 7 July 2006

Abstract

A new rare earth nickel stannide, Sm_2NiSn_4, has been prepared by reacting the pure elements at high temperature in welded tantalum tubes. Its crystal structure was established by single crystal X-ray diffraction studies. Sm_2NiSn_4 crystallizes in the orthorhombic space group *Pnma* (No. 62) with cell parameters of $a = 16.878(2)$ Å, $b = 4.4490(7)$ Å, $c = 8.915(1)$ Å, and $Z = 4$. Its structure can be viewed as the intermediate type between $ZrSi_2$ and $CeNiSi_2$. Sm_2NiSn_4 features two-dimensional (2D) corrugated $[NiSn_4]^{6-}$ layers in which the 1D Sn zigzag chains and the 2D Sn square sheets are bridged by Ni atoms. The Sm^{3+} cations are located at the interlayer space. Results of both resistivity measurements and extended-Hückel tight-binding band structure calculations indicate that Sm_2NiSn_4 is metallic.

Keywords: Polar intermetallics; Solid-state reaction; Crystal structure; Rare earth nickel stannide

1. Introduction

Intermetallic phases formed between alkali earth metal (or alkali metal or rare earth metal) and tin element are of great research interest due to their richness in structural chemistry and tunable electronic properties [1]. Phase diagram studies indicate that the Ca–Sn system alone exhibits seven intermediate phases [2,3]. Several types of anionic tin oligomers have also been found in these binary and ternary phases [2,4]. Mixing two types of cations with different sizes such as the combination of alkali earth and alkali metals, or two different alkali metals or two different alkali earth metals affords a number of polar intermetallics with unusual anionic clusters, chains and layers [5–8]. The tin-rich binary or ternary phases are also capable of forming type I clathrates featuring cages based on tin pentagons and possessing interesting transport properties [9].

The Pauling's electronegativities of Cu (1.90) and Ni (1.91) are very close to that of Sn (1.96), hence it is expected that a variety of *A*–Cu(Ni)–Sn (*A* is alkali earth, alkali or rare earth metal) ternary phases with strong covalent Cu(Ni)–Sn bonding can be formed. Furthermore, the introduction of the transition metals in these systems can also dramatically change the electronic and magnetic properties of the resultant intermetallic compounds as well as improve their thermal stabilities [1]. Rare earth copper stannides have been widely investigated due to their interesting magnetic and transport properties [10]. It is recently reported that the structure of $Ca_6Cu_2Sn_7$ features a novel three dimensional (3D) open framework built from $[Cu_2Sn_3]$ layers cross-linked by novel zigzag $[Sn_4]$ tetramers [11]. As for the Ae–Ni–Sn system, a few phases reported include $BaNiSn_3$, $Mg_{11.92}Ni_{2.32}Sn_{1.76}$, $MgNi_2Sn$ and $Ca_7Ni_4Sn_{13}$ [12]. It is interesting to mention that $Ca_7Ni_4Sn_{13}$ features a interesting 3D anionic network formed by 1D condensed chains of "drum"-like $[Ni_4Sn_4Sn_{8/2}]$ clusters interconnected by square planar $[Sn_5]$ units via *exo*-bonds was reported [12d]. A large number of rare earth nickel tin ternary phases have been isolated [13–19]. A few such compounds belong to the $RENi_{1-x}Sn_2$ family with the $CeNiSi_2$ structure type, the nickel site is normally partially occupied with the $1-x$ value in the range of 0.08–0.74 [13]. It also should be mentioned that $LuNiSn_2$ and $DyNiSn_2$ are not of the $CeNiSi_2$ structure type, but they form a new structure type which features Ni_2Sn_3 five member rings [14]. Besides some

*Corresponding author. Fax: +86 591 8371 4946.
E-mail address: mjg@ms.fjirsm.ac.cn (J.-G. Mao).

0022-4596/$ - see front matter © 2006 Elsevier Inc. All rights reserved.
doi:10.1016/j.jssc.2006.07.002

nickel-rich ternary phases, other rare earth nickel tin ternary compounds reported include RENiSn with the TiNiSi structure type [15], $CeNi_2Sn_2$ in the $CeAl_2Ga_2$ structure type [16], Lu_2NiSn_6 featuring layers of [$NiSn_4$] and 1D zigzag chains of 2-bonded Sn atoms and $LuNiSn_4$ composed of [$NiSn_3$] layers and 1D zigzag chains of 2-bonded Sn atoms [17], $Ce_3Ni_2Sn_7$ in the $La_3Co_2Sn_7$ structure [18], $La_{4.87}Ni_{12}Sn_{24}$ and $Gd_3Ni_8Sn_{16.33}$ [19]. Our attempts to prepare the rare earth nickel analogs of $Ca_6Cu_2Sn_7$ led to the discovery of a novel polar intermetallics phase, Sm_2NiSn_4. Its structure can be viewed as the intermediate type between $ZrSi_2$ and $CeNiSi_2$ structure types [13,20]. Herein, we report its syntheses, crystal structures, band structures, and physical properties.

2. Experimental section

2.1. Materials and instrumentation

All manipulations were performed inside an argon-filled glove box with moisture level below 1 ppm. The starting materials are samarium pieces (99.98%, Alfa-Aesar), nickel powder (99.999%, Tianjin Fuchen chemical reagent company), and tin granules (99.8%, Shanghai fourth chemical reagent company). DC magnetic measurement was performed on a PPMS-9T magnetometer at a field of 5000 Oe in the temperature range of 2–300 K. The resistivity measurements were performed on an Oxford Mablab-12 magnetometer by using a standard four-probe technique in the temperature range of 6–300 K. An energy dispersive X-ray spectroscope (EDS, Oxford INCA) analysis attached to the FESEM was used to analyze the elemental composition. X-ray powder diffraction patterns were collected on an X'Pert-Pro diffractometer using Cu$K\alpha$ radiation ($\lambda = 1.5406$ Å) in the 2θ range of 5–85°. The generator voltage is 45 kV and the tube current is 40 mA.

2.2. Syntheses of Sm_2NiSn_4

Single crystals of Sm_2NiSn_4 was initially obtained by reacting a mixture composed of Sm, Ni, and Sn in a molar ratio of 6:2:7 at 950 °C, in our attempts to prepare $Sm_6Ni_2Sn_7$, which could be an analog of $Ca_6Cu_2Sn_7$ [9]. A mixture of Sm (225.5 mg, 1.5 mmol), Ni (29.4 mg, 0.5 mmol) and Sn (209.3 mg, 1.75 mmol) was loaded into a niobium tube, which was subsequently arc-welded under an argon atmosphere and put into an evacuated quartz tube. The sample was allowed to heat at 950 °C for 5 days with prior heating under dynamic vacuum at 300 °C for 1 day. Then it was allowed to cool slowly (15 °C/h) to room temperature. Single crystals of Sm_2NiSn_4 (gray, plate-shaped) were obtained in low yield. Several single crystals were used for the microprobe elemental analyses. The measured chemical composition, $Sm_{1.92}Ni_{0.88}Sn_{4.0}$, is very close to the structurally refined one. After proper structural analyses, Sm_2NiSn_4 was prepared quantitatively by the reactions of the stoichiometric mixtures of the pure metals in Ta tubes at 970 °C for 36 h, quenched in water and annealed at 700 °C for 15 days. Sm_2NiSn_4 is air-stable and its purity was confirmed by X-ray powder diffraction studies (see Supporting Information). The use of the Ta tubes instead of the Nb tubes is to eliminate Nb_3Sn impurity found in the products when Nb tubes were used. Attempts to prepare other RE_2NiSn_4 analogies (RE = La, Gd, Yb) were tried but unsuccessful.

2.3. Crystal structure determination

A single crystal of Sm_2NiSn_4 (size: $0.15 \times 0.08 \times 0.05$ mm^3) was selected from the reaction products and sealed into a thin-walled glass capillary under an argon atmosphere. Data collection was performed on a Rigaku Mercury CCD (Mo$K\alpha$ radiation, graphite monochromator) at 293(2) K. The data set was corrected for Lorentz factor, polarization, air absorption and absorption due to variations in the path length through the detector faceplate. Absorption correction based on Multi-scan method was also applied [21a].

The structure of Sm_2NiSn_4 was solved by using direct methods (SHELXTL) and refined by least-squares methods with atomic coordinates and anisotropic thermal parameters [21b]. Based on systematic absences and E-value statistics, two space groups, $Pnma$ and $Pna2_1$ are possible for Sm_2NiSn_4, of which the centrosymmetric one gave a satisfactory refinement. All atomic sites in Sm_2NiSn_4 are fully occupied according to the site occupancy refinements and no abnormal behavior was found for their thermal parameters. Final difference Fourier maps showed featureless residual peaks of 2.29 and -2.28 e Å^{-3} (0.71 and 1.45 Å from Sn(2) and Sn(1), respectively). Crystallographic data and structural refinements are summarized in Table 1. Atomic coordinates, and selected bond lengths and angles are listed in Tables 2 and 3, respectively. More details about crystallographic studies are given as the Supporting Information. Crystallographic data in CIF format for Sm_2NiSn_4 has been deposited as CSD number 416584. These data may be obtained free of charge by contacting FIZ Karlsruhe at +49 7247 808 666 (fax) or crysdata@fiz-karlsruhe.de (email).

2.4. Extended hückel band calculations

Three-dimensional band structure calculations for Sm_2NiSn_4 along with the density of states (DOS) and crystal orbital overlap population (COOP) curves were performed by using the Crystal and Electronic Structure Analyzer (CAESAR) software package [22]. The following atomic orbital energies were employed for the calculations: Sm 6s −4.86, 6p −4.86, 5d −6.06, 4f −11.28; Ni 4s −9.17, 4p −5.15, 3d −13.49; Sn 5s −16.16, 5p −8.32 eV.

3. Results and discussion

Both $ZrSi_2$ and $CeNiSi_2$ crystallize in orthorhombic $Cmcm$ [20,23]. Comparing the cell parameters of the

Table 1
Summary of cell parameters, data collection and structure refinements for Sm_2NiSn_4

Empirical formula	Sm_2NiSn_4
fw	1198.39
Space group	*Pnma* (No. 62)
A, Å	16.878(2)
B, Å	4.4490(7)
C, Å	8.915(1)
V, Å^3	669.4(2)
Z	4
D_{calcd}, g cm^{-3}	8.277
Temp, K	293(2)
μ, mm^{-1}	34.544
Size (mm)	$0.15 \times 0.08 \times 0.05$
Color and habit	gray, plate
h k l range	(−21, 20), ±5, (−10, 11)
Reflections collected	4849
Unique reflections	861 ($R_{int} = 0.0416$)
Reflections ($I > 2\sigma(I)$)	781
GOF on F^2	1.057
R_1, wR_2 ($I > 2\sigma(I)$)[a]	0.0261/0.0680
R_1, wR_2 (all data)	0.0318/0.0707

$R_1 = \sum||F_o|-|F_c||/\sum|F_o|$, $wR_2 = \sum w[(F_o)^2 - (F_c)^2]^2/\sum w[(F_o)^2]^{21/2}$.

Table 2
Atomic coordinates and U(eq)(× 103 Å2) for Sm_2NiSn_4

Atom	Wyck.	*x*	*y*	*z*	U_{eq}
Sm(1)	4c	0.14807(3)	1/4	0.36580(5)	4(1)
Sm(2)	4c	0.35292(3)	3/4	0.39035(6)	5(1)
Ni(1)	4c	0.06200(9)	3/4	0.1438(1)	12(1)
Sn(1)	4c	0.32411(5)	1/4	0.12728(6)	8(1)
Sn(2)	4c	0.29041(5)	1/4	0.62914(6)	7(1)
Sn(3)	4c	0.99184(5)	1/4	0.12994(6)	7(1)
Sn(4)	4c	0.99180(5)	3/4	0.39000(7)	8(1)

$CeNiSi_2$ and Sm_2NiSn_4, it is noticed that $a_{Sm2NiSn4} \approx b_{CeNiSi2}$, $c_{Sm2NiSn4} \approx 2a_{CeNiSi2}$ and $b_{Sm2NiSn4} \approx c_{CeNiSi2}$. Since Sm_2NiSn_4 crystallizes in orthorhombic *Pnma* which is primitive, hence Sm_2NiSn_4 forms a different structure type from those of $ZrSi_2$ and $CeNiSi_2$.

The structure of Sm_2NiSn_4 features a 2D [$NiSn_4$] layer composed of Sn square sheet and zigzag Sn chains that are bridged by nickel atoms (Fig. 1). Such structure type is the intermediate version between $ZrSi_2$ and $CeNiSi_2$.

The 2D Sn square sheet is formed by Sn(3) and Sn(4) atoms (Fig. 2a). Half of the Sn_4 squares within the square sheet are capped by Ni atoms alternatively on both sides, resulting in [$NiSn_2$] layers. Within the [$NiSn_2$] layer, the distance from Ni(1) to the Sn_4 square is 1.123 Å. Such connectivity results in also 1D [NiSn] "ladder" composed of Ni(1) and Sn(3) along the *b*-axis, and these ladders are further bridged by Sn(4) atoms into a 2D architecture (Fig. 2a). It is interesting to note that such [NiSn] "ladder" is very similar to the [CuSn] one in $Ca_6Cu_2Sn_7$ (Fig. 2b) [11]. Within the [$NiSn_2$] layer, three types of Sn–Sn bonds are found: Sn(4)–Sn(4) (2.9785(9) Å) for the vacant [Sn_4] square composed of one Sn(3) and three Sn(4) atoms,

Table 3
Selected bond lengths (Å) and angles for Sm_2NiSn_4

Sm(1)–Sn(2)	3.2369(6) × 2	Sm(1)–Sn(1)	3.2561(6) × 2
Sm(1)–Sn(2)	3.3590(8)	Sm(1)–Sn(3)	3.3725(9)
Sm(1)–Sn(4)	3.4571(9) × 2	Sm(1)–Sn(1)	3.6537(9)
Sm(1)–Ni(1)	3.313(1) × 2	Sm(2)–Sn(3)	3.2371(8) × 2
Sm(2)–Sn(2)	3.2546(6) × 2	Sm(2)–Sn(1)	3.2687(6) × 2
Sm(2)–Sn(2)	3.3578(9)	Sm(2)–Sn(3)	3.3804(9)
Sm(2)–Sn(4)	3.4264(9)	Sm(2)–Ni(1)	3.481(1) × 2
Sm(2)–Ni(1)	3.542(2)	Ni(1)–Sn(4)	2.494(2)
Ni(1)–Sn(2)	2.494(2)	Ni(1)–Sn(3)	2.5231(9) × 2
Ni(1)–Sn(3)	2.604(2)	Sn(1)–Sn(2)	2.9470(8) × 2
Sn(3)–Sn(4)	3.2130(7) × 2	Sn(3)–Sn(3)	3.2236(9) × 2
Sn(4)–Sn(4)	2.9785(9) × 2		
Sn(4)–Ni(1)–Sn(2)	121.38(6)	Sn(4)–Ni(1)–Sn(3)	79.64(4) × 2
Sn(2)–Ni(1)–Sn(3)	117.78(3) × 2	Sn(3)–Ni(1)–Sn(3)	123.68(7)
Sn(4)–Ni(1)–Sn(3)	131.21(7)	Sn(2)–Ni(1)–Sn(3)	107.42(5)
Sn(3)–Ni(1)–Sn(3)	77.89(3) × 2	Ni(1)–Sn(4)–Sn(3)	50.58(2) × 2
Ni(1)–Sn(2)–Sn(1)	130.94(2) × 2	Ni(1)–Sn(3)–Ni(1)	123.68(7)
Ni(1)–Sn(3)–Ni(1)	102.11(3) × 2	Ni(1)–Sn(3)–Sn(4)	49.78(3) × 2
Ni(1)–Sn(3)–Sn(4)	125.11(4) × 2	Ni(1)–Sn(3)–Sn(4)	132.54(2) × 2
Ni(1)–Sn(3)–Sn(3)	52.17(3) × 2	Ni(1)–Sn(3)–Sn(3)	49.93(2) × 2
Ni(1)–Sn(3)–Sn(3)	127.12(4)	Ni(1)–Sn(4)–Sn(4)	122.36(4) × 2
Sn(4)–Sn(3)–Sn(3)	175.11(5) × 2	Sn(4)–Sn(3)–Sn(3)	92.34(2) × 2
Sn(3)–Sn(3)–Sn(3)	87.27(3)	Sn(2)–Sn(1)–Sn(2)	98.02(3) × 2
Sn(4)–Sn(4)–Sn(4)	96.64(4)	Sn(4)–Sn(3)–Sn(4)	87.63(2)
Sn(4)–Sn(4)–Sn(3)	172.83(4) × 2	Sn(4)–Sn(4)–Sn(3)	87.59(2) × 2
Sn(3)–Sn(4)–Sn(3)	87.63(2)		

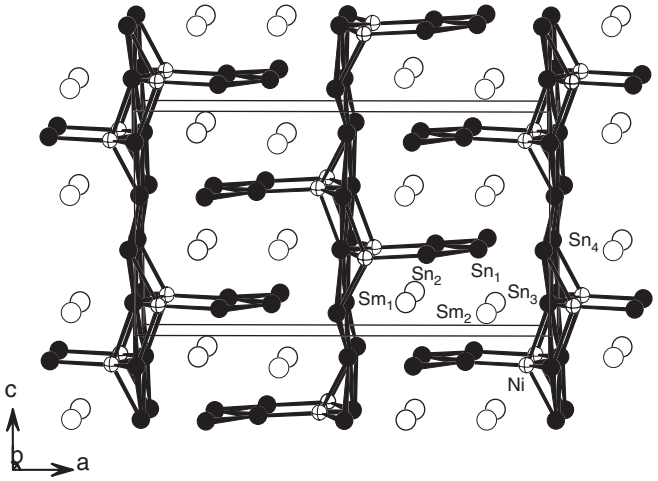

Fig. 1. View of the structure of Sm_2NiSn_4 down the *b*-axis.

Sn(3)–Sn(3) (3.2236(9) Å) for the Ni-capped [Sn_4] square, and Sn(3)–Sn(4) (3.2130(7) Å) which is shared by the above two types of squares. The Sn(4)–Sn(4) distance is significantly longer than the Sn–Sn single bond distance of 2.81 Å in the diamond modification of α–Sn [24]. The Ni-Sn distances fall in the range of 2.494(2)–2.604(2) Å, which are comparable with those in other rare earth nickel tin compounds [13–19]. It should be noted that the [$NiSn_2$] layer in Sm_2NiSn_4 is somehow similar to the [Cu_2Sn_3] layer in $Ca_6Cu_2Sn_7$ and the [NiSi] layer in $CeNiSi_2$ (Fig. 2) [11,23]. All of them feature a square sheet of tetrels (Si or Sn) capped by transition metals (Ni or Cu) alternatively

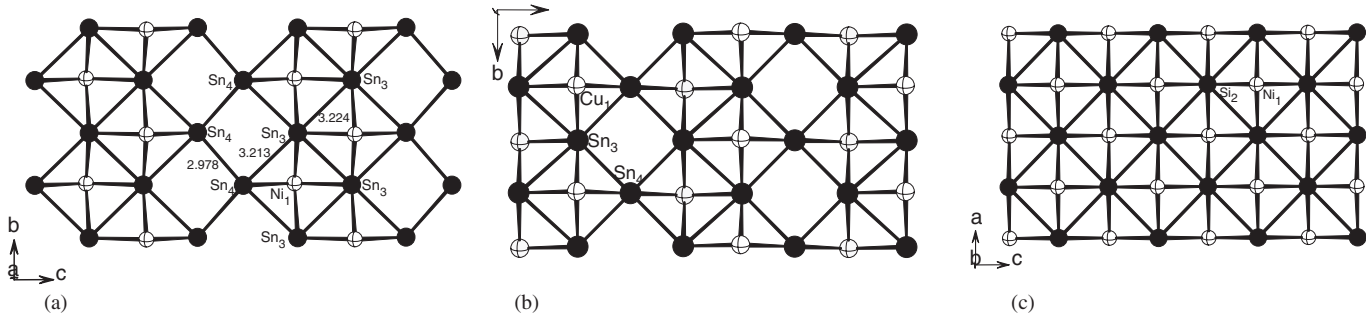

Fig. 2. Comparison of the $[NiSn_2]$ layer in Sm_2NiSn_4 (a) with the $[Cu_2Sn_3]$ layer in $Ca_6Cu_2Sn_7$ (b), and the [NiSi] layer in $CeNiSi_2$ (c).

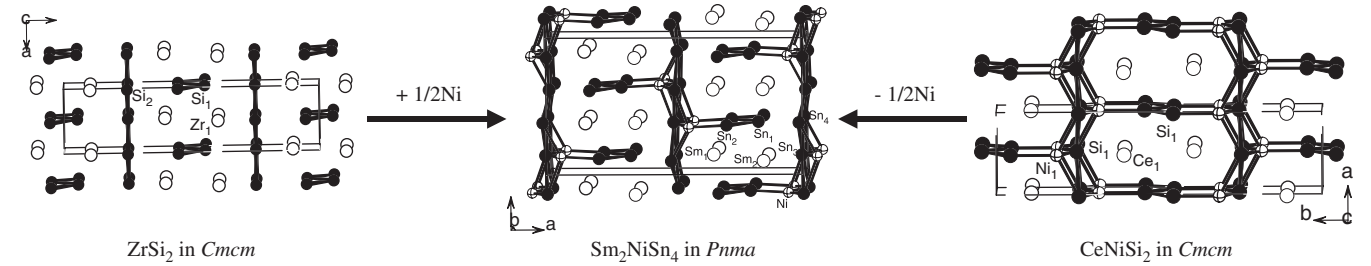

Fig. 3. Comparison of the structure of Sm_2NiSn_4 with those of $ZrSi_2$ and $CeNiSi_2$.

above and below. There are no vacant Si_4 squares in the [NiSi] layer, whereas half and one-third Sn_4 squares are vacant in the $[NiSn_2]$ and $[Cu_2Sn_3]$ layers, respectively (Fig. 2).

The zigzag Sn chain is formed by Sn(1) and Sn(2) atoms (Fig. 1), similar such tin chains can be found in Lu_2NiSn_6, $LuNiSn_4$, $ThSn_2$ and $AECuSn_2$ (AE = Sr, Ba) [17,25]. The Sn–Sn distance of 2.9470(8) Å is comparable to that in SrSn (2.924 Å) [26]. The Sn–Sn–Sn angle is 98.02(3)°, which is much smaller than that for an ideal tetrahedral geometry due to the presence of the lone pair electrons.

The above two types of building units in Sm_2NiSn_4 are further interlinked via Ni–Sn bonds (2.494(2) Å) into $[NiSn_4]$ layers (Fig. 1). Such $[NiSn_4]$ layer can also be viewed as being formed by $[NiSn_2]$ layer attached by 1D zigzag Sn chains alternatively on both sides. The shortest interlayer Sn…Sn separation is 3.603 Å. The Sm^{3+} cations are located at the interlayer space. Sm(1) is 11-coordinated by two Ni and nine Sn atoms, whereas Sm(2) is surrounded by three Ni and ten Sn atoms. The Sm–Ni and Sm–Sn distances are in the ranges of 3.313(1)–3.542(2) Å and 3.2369(6)–3.6537(9) Å, respectively. The Ni atom is in a distorted $[Sn_5]$ square pyramidal geometry. The Sn–Ni–Sn angles are in the range of 77.89(3) and 121.38(6)°.

It is very interesting to note that the structure of Sm_2NiSn_4 is closely related to the $ZrSi_2$ and $CeNiSi_2$ structure types [20,23]. As shown in Fig. 3, all three structures are based on 2D tetrel (Si or Sn) square sheets and 1D zigzag tetrel chains. The square sheets and the zigzag chains remain isolated in $ZrSi_2$. In $CeNiSi_2$, the silicon square sheets and zigzag chains are bridged by Ni atoms into a 3D open framework. As for Sm_2NiSn_4, the tin chains are only hanging on both sides of the $[NiSn_2]$ layer due to the lack of 50% Ni atoms compared with $CeNiSi_2$. Hence Sm_2NiSn_4 serves as an intermediate version between $ZrSi_2$ and $CeNiSi_2$ structural types. It should be mentioned that many phases in Ln–Ni–Sn system such as $LaNi_{0.74}Sn_2$ are nonstoichiometric and of the $CeNiSi_2$ structure type, in which the nickel site is only partially occupied [13].

It is also interesting to compare the structure of Sm_2NiSn_4 with those of Lu_2NiSn_6 and $LuNiSn_4$ [17]. All three compounds are composed of 2D tin square sheet with capping nickel atoms and 1D zigzag tin chains (Fig. 4). The 1D zigzag chains of tin in Sm_2NiSn_4 are bridged to the 2D tin square sheet through the capping nickel atoms whereas such 1D chains in Lu_2NiSn_6 and $LuNiSn_4$ are isolated. Furthermore, the nickel atom in Sm_2NiSn_4 is bonded to five tin atoms in a square pyramidal geometry whereas each nickel atom in Lu_2NiSn_6 and $LuNiSn_4$ is sandwich between two Sn_4 squares (Fig. 4), in other words, it is in the center of a Sn_8 cubane. Capping of the Ni atoms alternatively on both sides of the tin square sheet in Sm_2NiSn_4 resulted in the $[NiSn_2]$ layers. The interconnection of the nickel atoms and two tin square sheets in Lu_2NiSn_6 forms $[NiSn_4]$ double layers with the inter-sheet Sn–Sn distances of 3.151 and 3.216 Å, respectively (Fig. 4b). These inter sheet Sn–Sn bonds are slightly longer than those for the Sn_4 square (3.050 Å) [17]. In $LuNiSn_4$, three tin square sheets and the nickel atoms are interconnected into a $[NiSn_3]$ triple layers (Fig. 4c), and the Sn–Sn distances between two neighboring square sheets are 2.914 and 2.954 Å, respectively, which are slightly shorter than the Sn–Sn bonds within the tin square

(3.083 Å) [17]. The shortest Sn…Sn separations between the 1D tin chain and 2D nickel-tin layer are 3.563 and 3.654 Å, respectively, for Lu_2NiSn_6 and $LuNiSn_4$.

To obtain further insights into the chemical bonding of Sm_2NiSn_4, three dimensional band structure calculations were performed by using the semi-empirical extended Hückel methods [22]. Sm_2NiSn_4 is metallic with no band gap around the Fermi level (Fig. 5). The states just below and above the Fermi level are mainly from *p* orbitals of Sn atoms, mixing with small amount of *s* and *p* orbitals of Ni atoms, as well as small amount of *s* and *p* contributions from Sm atoms. The two peaks in the DOS, observed around the Fermi level and −2.0 eV, are the results of splitting of Sm *f* and Ni *d* states due to spin-orbit interactions, respectively. E_F suggests that Sm *f* states are partially occupied. This indicates the f^5 electron configuration corresponding to Sm^{3+}, which is in agreement with the results of magnetic measurements. However, the Ni *d* orbitals are almost fully occupied with eletrons below the Fermi level, indicating a reduced state for Ni(1) atom. This is reasonable, as is well known that, in many intermetallic phases containing late transition metals with high electronegativity, band structure calculations suggest the transition metals are effectively in neutral or negative oxidation states [11,27]. Semi-empirical COOP allows a more quantitative bond analysis. The Sn–Sn bond (2.9470(8) Å) of the zigzag Sn chain has an overlap population (OP) value of 0.274, which is much stronger than the Sn–Sn bonds (average OP = 0.174) of the [$NiSn_2$] layer. The Ni–Sn bonds (2.494–2.604 Å) with an average OP value of 0.345 are significant bonding. The Sm–Sn (3.2369(6)–3.6537(9) Å) and Sm–Ni (3.313(1)–3.542(2) Å) bonds with small OP values of 0.049 and 0.022, respectively, are very weak bonding.

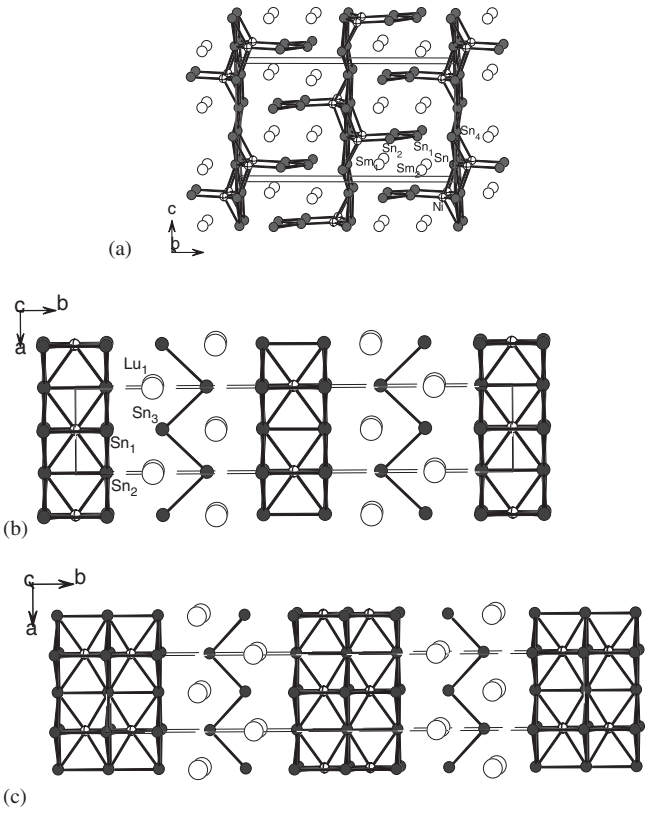

Fig. 4. Comparison of the structure of Sm_2NiSn_4 (a) with those of Lu_2NiSn_6 (b) and $LuNiSn_4$ (c).

The magnetic susceptibility of Sm_2NiSn_4 measured in the range of 2–300 K, is shown in Fig. 6a. It does not obey the Curie–Weiss law over the entire experimental temperature region. The sharp maximum of the χ_M–*T* plot at 17 K indicates that it undergoes an antiferromagnetic ordering transition at low temperature. The calculated effective moment μ_{eff} is 1.81 μ_B/Sm-atom at 300 K, which is slightly higher than the theoretical values of 1.66 μ_B for one Sm^{3+} ion per formula based on the Van Vleck formula [28]. Resistivity measurements reveal a metallic behavior for Sm_2NiSn_4 with $\rho_{298} = 75.5\,\mu\Omega\,cm$ and $\rho_6 = 53.7\,\mu\Omega\,cm$, respectively (Fig. 6b). There is an obvious transition near the Néel temperature (ca. 17 K), which is in good agreement with the magnetic data. These values are comparable to those for $RE_9Ni_{24}Sn_{49}$ phases (*RE* = Y, Ce, Pr, Sm and Tb) [29].

In summary, we have obtained a novel rare earth tin-rich ternary phase Sm_2NiSn_4. The structure of Sm_2NiSn_4 features a 2D anionic [$NiSn_4$] layer in which 1D Sn zigzag

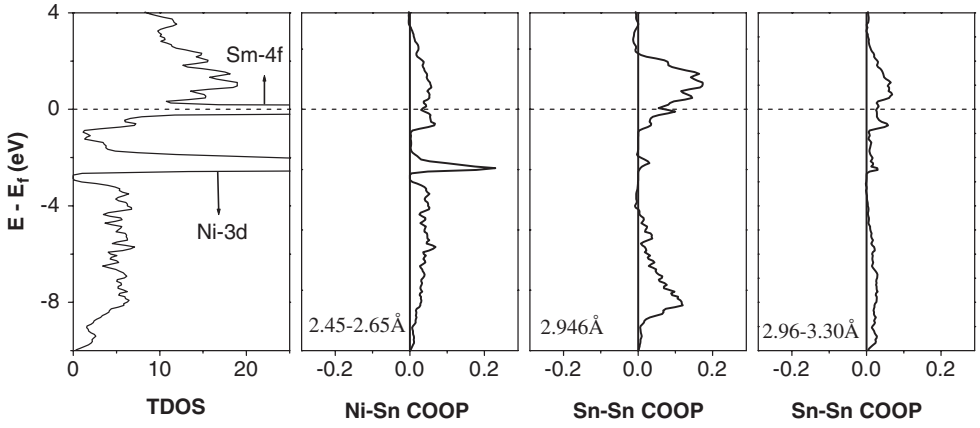

Fig. 5. DOS and COOP curves for Sm_2NiSn_4. The Fermi level is represented by the dotted line and is set at 0 eV.

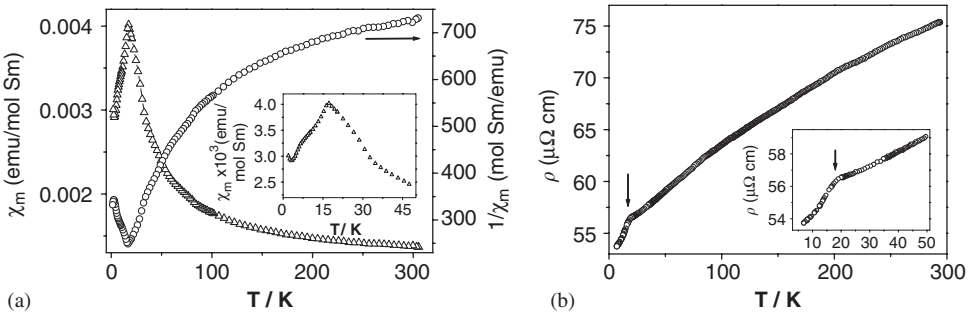

Fig. 6. χ_m and χ_m^{-1} versus T plots (a) and the dependences of ρ with temperature for Sm_2NiSn_4 (b). The inset shows magnified view at low temperatures.

chains and 2D Sn square sheets are interconnected by bridging Ni atoms. It is the intermediate type between $ZrSi_2$ and $CeNiSi_2$. Sm_2NiSn_4 is metallic based on band structure calculation as well as resistivity measurements.

4. Supporting information available

Figures showing the coordination geometries around Sm, Sn and Ni atoms, lists of atomic displacement parameters, simulated and experimental XRD powder patterns.

Acknowledgments

We thank the financial supports from the Nation Natural Science Foundation of China (No. 20573113, 20371047 and 20521101) and NSF of Fujian Province (No. E0420003). We thank Prof. Shunlian Jia for her help with the resistivity measurements.

Appendix A. Supplementary materials

Supplementary data associated with this article can be found in the online version at doi:10.1016/j.jssc.2006.07.002.

References

[1] (a) B. Eisenmann, G. Cordier, Chemistry, Structure and Bonding of Zintl Phases and Ions, VCH Publishers, New York, 1996, p. 61;
(b) J.D. Corbett, Chemistry, Structure and Bonding of Zintl Phases and Ions, VCH Publishers, New York, 1996, p.139;
(c) J.D. Corbett, Angew. Chem. Int. Ed. 39 (2000) 670.
[2] (a) A. Palenzona, P. Manfrinetti, M.L. Fornasini, J. Alloys Compd. 312 (2000) 165;
(b) E. Zintl, S. Neumayr, Z. Elektrochem. 39 (1933) 86;
(c) P. Eckerlin, H.J. Meyer, E. Wölfel, Z. Anorg. Allg. Chem. 281 (1955) 322;
(d) A.K. Ganguli, A.M. Guloy, E.A. Leon-Escamilla, J.D. Corbett, Inorg. Chem. 32 (1993) 4349.
[3] (a) A.M. Guloy, J.D. Corbett, Z. Anorg. Allg. Chem. 616 (1992) 61;
(b) E.A. Leon-Escamilla, J.D. Corbett, J. Alloys Compd. 265 (1998) 104;
(c) P. Eckerlin, E. Leicht, E. Wölfel, Z. Anorg. Allg. Chem. 307 (1961) 145.
[4] E.A. Leon-Escamilla, J.D. Corbett, Inorg. Chem. 38 (1999) 738.
[5] (a) I. Todorov, S.C. Sevov, Inorg. Chem. 43 (2004) 6490;
(b) S. Bobev, S.C. Sevov, J. Alloy Compd. 338 (2002) 87;
(c) S. Bobev, S.C. Sevov, J. Am. Chem. Soc. 124 (2002) 3359;
(d) S. Bobev, S.C. Sevov, Inorg. Chem. 40 (2001) 5361.
[6] (a) S. Bobev, S.C. Sevov, Inorg. Chem. 39 (2000) 5930;
(b) S. Bobev, S.C. Sevov, Angew. Chem. Int. Ed. 39 (2000) 4108.
[7] B. Eisenmann, H. Schäfer, Z. Anorg. Allg. Chem. 403 (1974) 163.
[8] A.K. Ganguli, J.D. Corbett, M. Köckerling, J. Am. Chem. Soc. 120 (1998) 1223.
[9] (a) A.P. Wilkinson, C. Lind, R.A. Young, S.D. Shastri, P.L. Lee, G.S. Nolas, Chem. Mater. 14 (2002) 1300;
(b) C.W. Myles, J.J. Dong, O.F. Sankey, Phys. Rev. B 64 (2001) Art. No. 165202;
(c) S. Bobev, S.C. Sevov, J. Solid State Chem. 153 (2000) 92;
(d) G.S. Nolas, B.C. Chakoumakos, B. Mahieu, G.J. Long, T.J.R. Weakley, Chem. Mater. 12 (2000) 1947;
(e) G.S. Nolas, T.J.R. Weakley, J.L. Cohn, Chem. Mater. 11 (1999) 2470.
[10] (a) M.L. Fornasini, G. Zanicchi, D. Mazzone, P. Riani, Z. Kristallogr. NCS 216 (2001) 21;
(b) M.L. Fornasini, P. Manfrinetti, D. Mazzone, P. Riani, G. Zanicchi, J. Solid State Chem. 177 (2004) 1919;
(c) A. Szytula, D. Fus, B. Penc, A. Jezierski, J. Alloy Compd. 317–318 (2001) 340;
(d) W. Dörrscheidt, G. Savelsberg, J. Stöhr, H. Schäfer, J. Less-Common Metals 83 (1982) 269.
[11] Z.-M. Sun, S.-Q. Xia, Y.-Z. Huang, L.-M. Wu, J.-G. Mao, Inorg. Chem. 44 (2005) 9242.
[12] (a) W. Dörrscheidt, H. Schäfer, J. Less-Common Metals 58 (1978) 209;
(b) P. Rahlfs, Metallwirtschaft 16 (1937) 640;
(c) M. Boudard, B. Doisneau, F. Audebert, J. Alloys Compd. 370 (2004) 169;
(d) D.A. Vennos, M.E. Badding, F.J. Disalvo, J. Less-Common Metals 175 (1991) 339.
[13] (a) W. Dörrscheidt, G. Savelsberg, J. Stöhr, H. Schäfer, J. Less-Common Metals 83 (1982) 269;
(b) A. Gil, B. Penc, S. Baran, J. Hernandez-Velasco, A. Szytula, A. Zygmunt, J. Alloys Compd. 361 (2003) 32;
(c) P. Schobinger-Papamantellos, J. Rodriguez-Carvajal, G.H. Nieuwenhuys, L.W.F. Lemmens, K.H.J. Buschow, J. Alloys Compd. 262 (1997) 335;
(d) P. Schobinger-Papamantellos, J. Rodriguez-Carvajal, H.F.J. Buschow, J. Alloys Compd. 240 (1996) 85.
[14] (a) L.P. Komarovskaya, L.G. Aksel'drud, R.V. Skolozdra, Kristallogr 28 (1983) 1201;
(b) L. Romaka, B. Penc, S. Baran, J. Leciejewicz, A. Szytuła, N. Stüsser, J. Hernandez-Velasco, A. Zygmunt, J. Alloys Compd. 343 (2002) 66.
[15] D. Rossi, R. Marazza, R. Ferro, J. Less-Common Metals 107 (1985) 99.

[16] R.V. Skolozdra, V.M. Mandzyk, Yu.K. Gorelenko, V.D. Tkachuk, Fiz. Met. Metalloved. 52 (1981) 966.
[17] (a) R.V. Skolozdra, L.G. Aksel'rud, O.E. Koretskaya, L.P. Komarovskaya, Dopov. Akad.i Nauk Ukr. RSR, Ser. B: Geol. Khim. Biol. Nauki 1985 (1985) 24;
(b) R.V. Skolozdra, J.S. Mudryk, L.G. Aksel'rud, D. Fruchart, D. Gignoux, J. Pierre, J. Alloys Compd. 296 (2000) 303.
[18] P. Schobinger-Papamantellos, G. Andre, J. Rodriguez-Carvajal, K.H.J. Buschow, L. Durivault, J. Alloys Compd. 325 (2001) 29.
[19] (a) M.A. Zhuravleva, D. Bilc, S.D. Mahanti, M.G. Kanatzidis, Z. Anorg. Allg. Chem. 629 (2003) 327;
(b) L.P. Komarovskaya, R.V. Skolozdra, Dopov. Akad. Nauk Ukr. RSR, Ser. A: Fiz.-Mat. Tekh. Nauki 47 (1985) 81.
[20] G.M. Zatorska, G.S. Dmytriv, V.V. Pavlyuk, E. Bartoszak-Adamska, M. Jaskolski, J. Alloys Compd. 346 (2002) 154.
[21] (a) CrystalClear ver. 1. 3. 5. Rigaku Corp., Woodlands, TX, 1999;
(b) G.M. Sheldrick, SHELXTL, version 5.03, Siemens Analytical X-ray Instructuments, Madison, WI, 1995;
(c) G.M. Sheldrick, SHELX-96 Program for Crystal Structure Determination, 1996.
[22] J. Ren, W. Liang, M.-H. Whangbo, CAESAR for windows, Prime-Color Software, Inc., North Carolina State University, Raleigh, NC, 1998.
[23] O.I. Bodak, E.I. Gladyshevskii, Kristallogr 14 (1969) 990.
[24] J. Donohue, The Structures of the Elements, Wiley, New York, 1974.
[25] (a) S. Cirafici, A. Palenzona, P. Manfrinetti, J. Less-Common Metals 90 (1983) 49;
(b) N. May, H. Schäfer, Z. Naturforsch. B 29 (1974) 20.
[26] (a) A. Palenzona, P. Manfrinetti, M.L. Fornasini, J. Alloys Compd. 312 (2000) 165;
(b) F. Merlo, M.L. Fornasini, J. Less-Common Metals 13 (1967) 603.
[27] B. Sieve, X. Chen, J. Cowen, P. Larson, S.D. Mahanti, M.G. Kanatzidis, Chem. Mater. 11 (1999) 2451.
[28] J.H. Van Vleck, The Theory of Electric and Magnetic Susceptibilities, Oxford University Press, London, 1932, p. 248.
[29] D. Kaczorowski, K. Gofryk, L. Romaka, Y. Mudryk, M. Konyk, P. Rogl, Intermetallics 13 (2005) 484.